

50  
NATIONAL AERONAUTICS AND SPACE ADMINISTRATION

*Technical Report 32-1114*

*Electronics for a Martian Water Vapor  
Detection System*

*John R. Locke*

JET PROPULSION LABORATORY  
CALIFORNIA INSTITUTE OF TECHNOLOGY  
PASADENA, CALIFORNIA

August 15, 1967

**N67-34759**

FACILITY FORM 602

(ACCESSION NUMBER)

(THRU)

19  
(PAGES)

1  
(CODE)

(NASA CR OR TMX OR AD NUMBER)

14  
(CATEGORY)


NATIONAL AERONAUTICS AND SPACE ADMINISTRATION

*Technical Report 32-1114*

*Electronics for a Martian Water Vapor  
Detection System*

*John R. Locke*

Approved by:

  
Harold R. Lawrence, Manager  
Lunar and Planetary Instruments Section

JET PROPULSION LABORATORY  
CALIFORNIA INSTITUTE OF TECHNOLOGY  
PASADENA, CALIFORNIA

August 15, 1967

**TECHNICAL REPORT 32-1114**

Copyright © 1967

Jet Propulsion Laboratory  
California Institute of Technology

Prepared Under Contract No. NAS 7-100  
National Aeronautics & Space Administration

PRECEDING PAGE BLANK NOT FILMED.

### **Acknowledgment**

I would like to thank and acknowledge Howard Marshall and Tim Harrington, who originally conceived of this method of measuring the capacitance of the aluminum oxide detector; Henry Mertz, for his many constructive ideas and helpful criticisms; and Gil Schuler, who has provided the necessary support in getting the ideas from the conceptual state to a working instrument.

## Contents

<b>I. Introduction</b>	1
<b>II. General Description of the System</b>	1
<b>III. Theory of Operation and Performance</b>	3
A. Water Vapor Concentration and Frequency	3
B. Performance vs Temperature	8
C. Processing the Error Signal	10
D. The Power Supply	11
<b>IV. Conclusion</b>	13
<b>Nomenclature</b>	14

## Tables

1. Experimental data and corresponding frequencies	7
2. Variations of $\gamma$ as a function of frequency	7
3. Instrument calibration and frequency deviation as a function of temperature	8
4. The repeatability of frequency deviation vs temperature	9

## Figures

1. The Martian water vapor detection system	2
2. Typical aluminum oxide calibration curve of frost/dew point vs impedance	3
3. Simplified block diagram of the water vapor detection system	4
4. Aluminum oxide water-detection electronics	5
5. Theoretical and measured capacitance–frequency relationships	6
6. Frequency and $H$ as a function of control voltage	7
7. Thermal characteristics of the VCO frequency control diodes	8
8. The Wien bridge oscillator	10
9. Bridge circuit and vector diagram	10
10. Water-detection power conversion and regulator system	12
11. Converter (dc to ac)	13
12. Simplified diagram of the voltage regulator	13

## **Abstract**

The electronic circuitry described in this report was developed to complement an aluminum oxide detector of high sensitivity which has been proposed for investigating the water content of the Martian atmosphere and/or surface. The detector and electronics constitute an instrument that has many advantages, some of which are small size (less than 36 in.<sup>3</sup>), light weight (approximately 0.8 lb), low power requirements (less than 0.4 W), and digital data output without the need of an analog-to-digital converter.

The theory of operation is described qualitatively, and a quantitative relationship is developed between water vapor concentration and the output signal of the instrument. The effects of temperature are treated and a brief analysis of the system power supply is discussed.

# Electronics for a Martian Water Vapor Detection System

## I. Introduction

The electronics described in this report were developed to complement a water vapor detector of high sensitivity which has been proposed for investigating the water content of the Martian atmosphere and/or surface.<sup>1</sup>

The detector, which was developed and is manufactured by Parametrics, Incorporated, of Waltham, Massachusetts, consists of a thin sheet of aluminum that is anodized by a special procedure to provide a porous oxide coating. A gold layer is evaporated on the oxide to form the outer electrode. The element senses absolute water vapor concentration. For low water vapor concentrations, the detector has the property of a capacitor whose capacitance changes as a function of the water vapor present.

Because data processing can be accomplished most conveniently and efficiently from the science instruments in digital form, the aluminum oxide water detector is utilized as one element of a bridge circuit. When the bridge circuit is driven at the appropriate frequency, the reactance of the detector is the proper value to balance the bridge. By monitoring this frequency, or cor-

responding count rate, one can determine the capacitance of the detector and thereby know the water vapor concentration. This technique has the advantage of not requiring an analog-to-digital converter and thereby saves weight, volume, and power.

The material of this report has been organized, first, to describe the general nature and function of the system qualitatively. This description is followed by an analysis of some of the more significant design considerations.

## II. General Description of the System

Figure 1 is a block diagram of the proposed Martian water vapor detection system, which can best be characterized as a null-seeking device. The bridge circuit, which contains the water vapor detector, whose capacitance is  $C_x$ , is of principal importance in determining the key performance characteristics of the system, such as sensitivity and frequency range. Considering the bridge as two divider networks, one composed of  $R_{22}$  and  $R_{23}$ , the other being  $C_x$  and  $R_{21}$ , it becomes apparent that for the amplitudes of the two signal voltages  $e_s$  and  $e_R$  to remain equal, the reactance of the aluminum oxide detector must be a constant. Since the capacitance of the detector changes as a function of water vapor, the frequency of the signal driving the bridge ( $e_o$ ) must vary inversely with the changing capacitance.

<sup>1</sup>Franzgrote, E. J., and Ghleck, D. J., internal communication to the National Aeronautics and Space Administration on the measurement of water vapor on Mars by the aluminum oxide method, Jet Propulsion Laboratory, August 2, 1965.





power required by the water detection electronics is extremely small (125 mW), the power supply is inherently inefficient. The overall efficiency for the current limiter, power converter, and voltage regulator is approximately 32%. The worst deviation for either of the two output voltages, when changing the input voltage from 21 to 47 V, is 8 mV or 0.044%. Over the temperature range of  $-60$  to  $+100^\circ\text{C}$ , the temperature coefficient of regulation is  $0.002\%/^\circ\text{C}$  or better. The current limiter limits the maximum current to 60 mA.

### III. Theory of Operation and Performance

The material that follows will deal more specifically with the theory of operation and performance. The areas to be discussed will include the following:

- (1) The relationship between water vapor concentration and frequency.
- (2) The performance of the electronics as a function of temperature.
- (3) The method used in processing the error signal from the bridge circuit.
- (4) Design considerations in the power supply.

#### A. Water Vapor Concentration and Frequency

In this section the theoretical relationship between water vapor concentration and frequency will be developed, discussed, and compared with measured results.

Figure 2 shows the relationship of the impedance of a typical detector vs frost/dew point.<sup>2</sup> The accuracy of the calibration is repeatable to  $\pm 2^\circ\text{C}$  and the curve is linear for frost points below  $-20^\circ\text{C}$ . In the linear portion of the curve, the impedance of the detector is similar to pure capacitive reactance. Since the frequency at which the calibration was made is known to be 200 cps, the impedance may be written in terms of its capacitance, as is shown in Fig. 2. Because the curve is linear in the region of interest, Eq. (1) can be written as

$$F = -1.83 \times 10^{-7} \text{ pF} \times ^\circ\text{C} \frac{1}{C_x} + 7^\circ\text{C} \quad (1)$$

<sup>2</sup>Potential Planetary Atmosphere Sensors: The Kryptonate Oxygen Detector and the Aluminum Oxide Hygrometer, Final Report, JPL Contract 950684. Parametrics, Inc., Waltham, Mass., Dec. 1964.

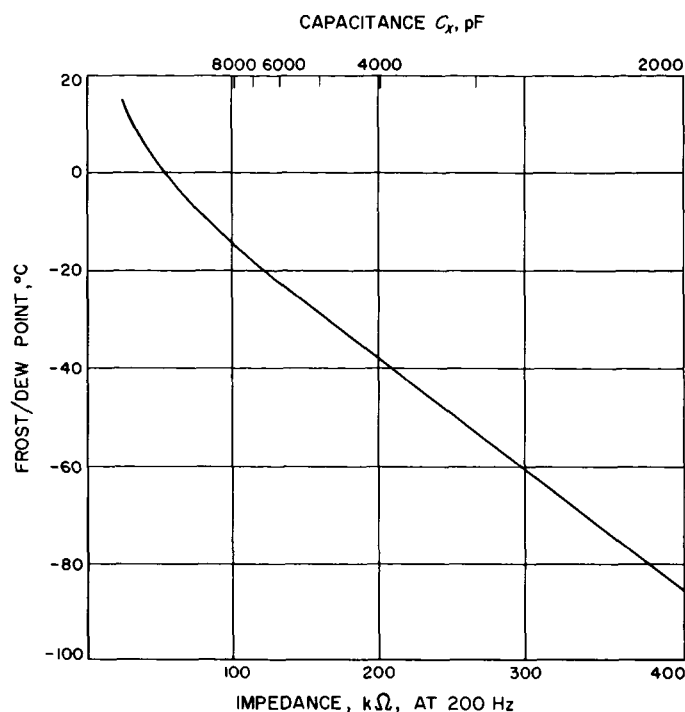


Fig. 2. Typical aluminum oxide calibration curve of frost/dew point vs impedance

(for  $F < -20^\circ\text{C}$ ), where  $F$  is the frost/dew point in  $^\circ\text{C}$  and  $C_x$  is the capacitive value of the aluminum oxide detector in picofarads.

Having established a relationship between the dew point and capacitance for this particular detector, a relationship will now be established between capacitance  $C_x$  values in the bridge circuit of the water vapor detection instrument and corresponding frequencies.

To aid in this discussion, Fig. 1 has been redrawn and simplified as Fig. 3, with appropriate notations to clarify references that will be made in the development of the capacitance-frequency relationship. Figure 4 is a schematic of the actual circuit.

Assuming that  $H$  is a linear transfer function relating output frequency ( $\omega$  in radians per second) to input control voltage  $V_c$  (in volts), then

$$\omega = H V_c \quad (2)$$

where

$$V_c = V_o + A_2 \epsilon \quad (3)$$

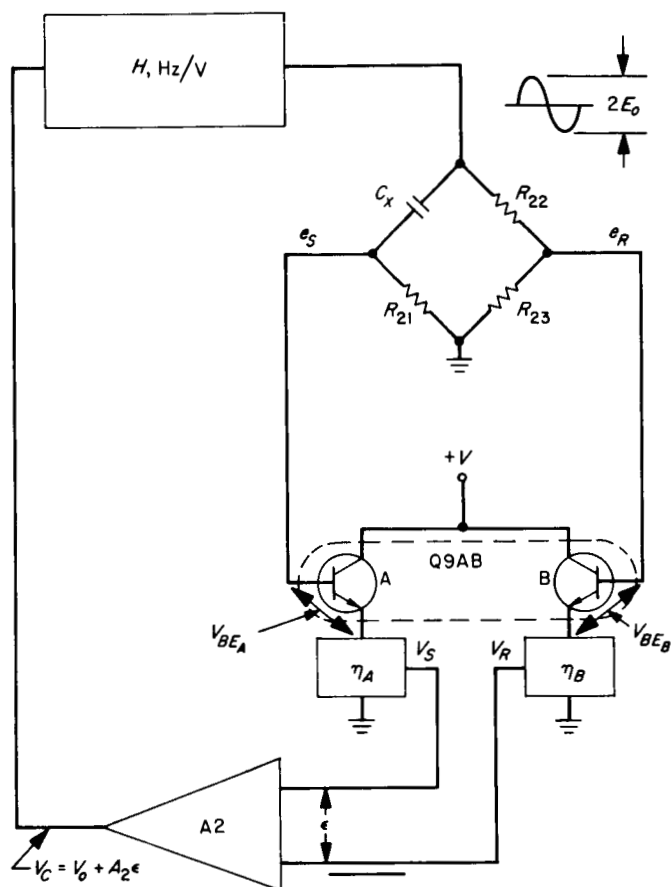


Fig. 3. Simplified block diagram of the water vapor detection system

and  $V_o$  is the voltage the differential amplifier's output would be if the differential input voltage were zero, while  $A_2$  is the voltage gain of the differential amplifier, and  $\epsilon$  is the error signal input to the differential amplifier.

The error signal can be expressed as

$$\epsilon = (K_R E_o - V_{BE_B}) \eta_B - (K_S E_o - V_{BE_A}) \eta_A \quad (4)$$

where

$$K_R = \frac{R_{23}}{R_{22} + R_{23}}$$

$E_o$  = peak output voltage from the ac amplifier A1, which drives the bridge circuit containing  $C_x$

$V_{BE_A}, V_{BE_B}$  = the base-emitter voltages of transistors A and B of Q9 and are approximately equal to 0.6 V for a silicon transistor.

$$\eta_A = \frac{V_S}{e_{S_{max}} - V_{BE_A}}, \eta_B = \frac{V_R}{e_{R_{max}} - V_{BE_B}}$$

$K_S$  = the divider ratio fixed by the aluminum oxide detector and resistor  $R_{21}$ , and is expressed as

$$\frac{\omega R_{21} C_x}{[(\omega R_{21} C_x)^2 + 1]^{1/2}}$$

In order to greatly simplify the mathematics, advantage will be taken of the fact that the reactance of the detector ( $C_x$ ) is maintained approximately constant. On the basis of this consideration,  $K_S$  will be written as

$$K_S = \frac{\omega R_{21} C_x}{\gamma} \quad (5)$$

where

$$\gamma = [(\omega R_{21} C_x)^2 + 1]^{1/2}$$

will be assumed a constant.

Substituting Eq. (5) into (4), (4) into (3) and (3) into (2) results in

$$\omega = H \{ V_o + A_2 [(K_R E_o - V_{BE_B}) \eta_B - (K_S E_o - V_{BE_A}) \eta_A] \}$$

Rearranging and solving for  $\omega$  yields

$$\omega = \frac{H[V_o + A_2 (K_R \eta_B E_o + \eta_A V_{BE_A} - \eta_B V_{BE_B})]}{1 + \frac{H A_2 \eta_A E_o R_{21} C_x}{\gamma}} \quad (6)$$

To gain more insight into the operation of the system, some simplifying approximations are in order. First it may be assumed that  $\eta_A = \eta_B$  and that  $V_{BE_A} = V_{BE_B}$ , which allows Eq. (6) to be written as

$$\omega = \frac{H(V_o + A_2 K_R \eta_B E_o)}{1 + \frac{H A_2 \eta_B E_o R_{21} C_x}{\gamma}} \quad (7)$$

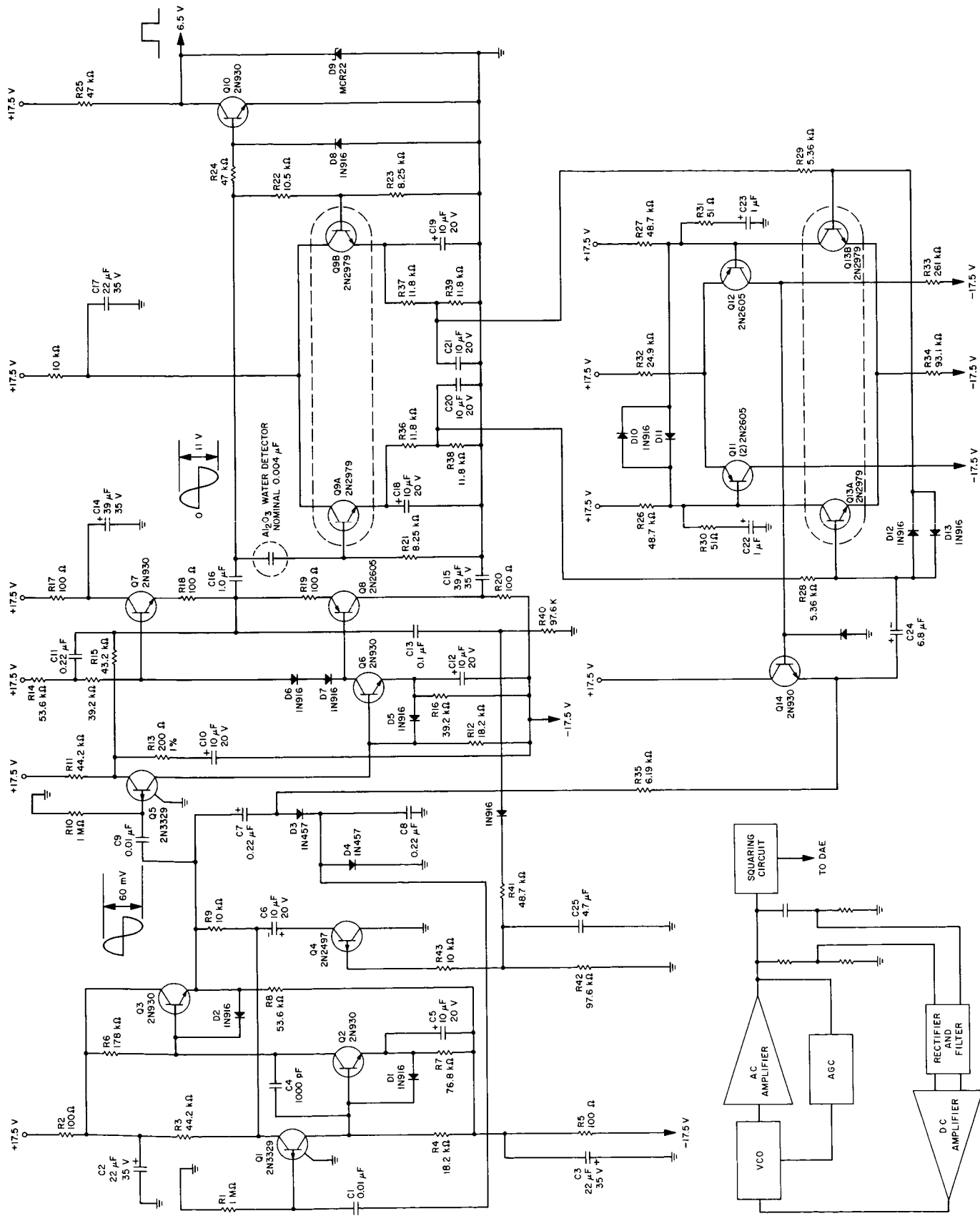


Fig. 4. Aluminum oxide water-detection electronics

Assigning typical values to the quantities in Eq. (7), such as

$$H = 640 \text{ Hz/V}$$

$$A_2 = 10,000$$

$$\eta_B = 0.5$$

$$E_o = 5.5 \text{ V}$$

$$R_{21} = 8.25 \text{ k}\Omega$$

$$C_x = 4000 \text{ pF}$$

$$V_o = 3.0 \text{ V}$$

$$K_R = 0.45$$

$$\gamma = 1.12$$

it can be seen that

$$1 + \frac{HA_2 \eta_B E_o R_{21} C_x}{\gamma} \approx \frac{HA_2 \eta_B E_o R_{21} C_x}{\gamma}$$

which allows Eq. (7) to be written as

$$\omega = \frac{\gamma}{R_{21} C_x} \left( \frac{V_o}{HA_2 \eta_B E_o} + K_R \right) \quad (8)$$

Again substituting the typical values listed, observe that

$$K_R \gg \frac{V_o}{HA_2 \eta_B E_o}$$

which allows a final expression of  $\omega$  to be written in terms of  $C_x$ , that is, in the relatively simple form of

$$f = \frac{\omega}{2\pi} = \frac{\gamma K_R}{2\pi R_{21} C_x} \quad (9)$$

By substituting the typical values listed earlier, Eq. (9) can be written

$$f = \frac{9.850 \times 10^{-6} \text{ Hz pF}}{C_x} \quad (10)$$

where  $C_x$  is in picofarads.

Figure 5 is a plot of Eq. (10) and data taken from a breadboard circuit, whose component values are those shown in Fig. 4. A decade capacitance box was used to simulate the capacitance of the aluminum oxide detector

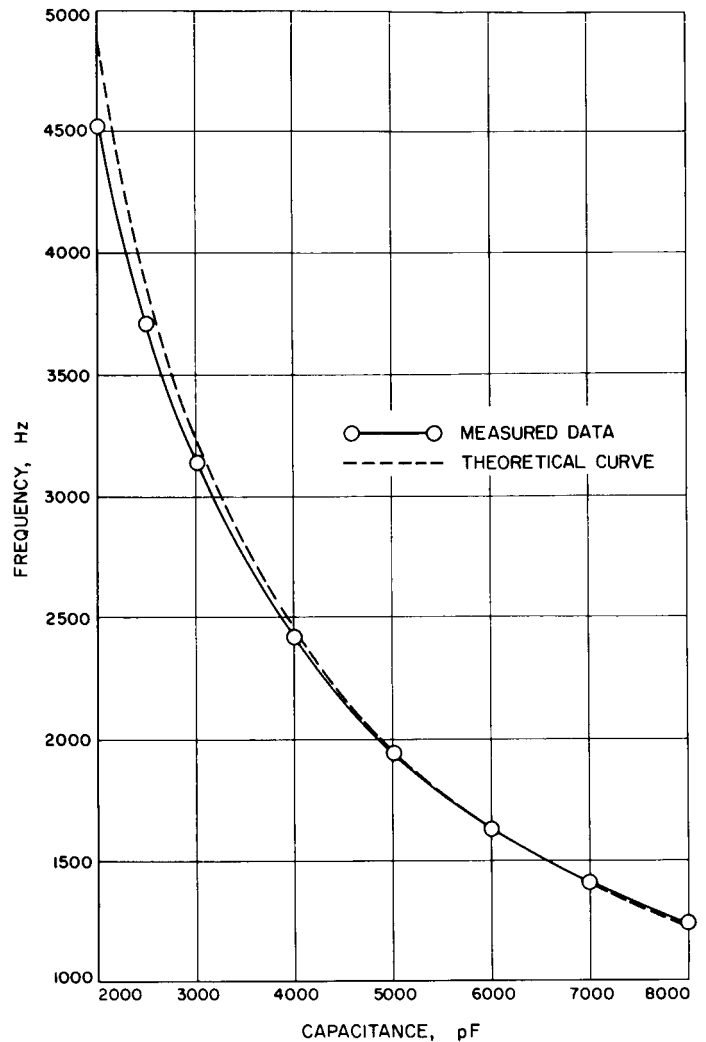


Fig. 5. Theoretical and measured capacitance-frequency relationships

for the data taken. Table 1 gives the experimental data plotted and the corresponding frequencies calculated from Eq. (10). These results indicate that the actual curve is in good correlation with the idealized theoretical curve and that a linear relationship will exist between frequency and frost point. This can be shown when Eq. (1) is combined with Eq. (10), resulting in

$$F = 18.5 \times 10^{-3} \text{ }^{\circ}\text{C/Hz} f + 7^{\circ}\text{C} \quad (11)$$

The noted deviation between the theoretical and measured results can largely be accounted for by (1) decreasing loop gain as a function of increasing frequency and (2) the inaccuracy of the assumption that the  $\gamma$  term, occurring in Eq. (9), is a constant.

**Table 1. Experimental data and corresponding frequencies**

$C_x$ , pF	Frequency, Hz		Percentage deviation $\left( \frac{f_c - f_M}{f_M} 100 \right)$
	Measured ( $f_M$ )	Calculated ( $f_c$ )	
2029.6	4520	4852	+7.4
2530.8	3710	3892	+4.9
3037.5	3140	3242	+3.3
4016.0	2415	2453	+1.6
5045.2	1942	1952	+0.52
6041.4	1633	1631	-0.12
7031.3	1410	1401	-0.64
8041.5	1238	1225	-1.1

Referring to Eq. (7), the loop gain of the system is given by

$$\frac{HA_2 \eta_B E_o R_{21} C_x}{\gamma} \triangleq G \quad (12)$$

From Table 1, observe that when the frequency changes from 1238 to 4520 Hz, the capacitance of  $C_x$  decreases by a factor of four; thus the loop gain  $G$  is decreased to one-quarter of its original value.

In the derivation of the frequency expression (Eq. 9), the assumption was made that the transfer function  $H$  of the voltage-controlled oscillator was a constant, and, this being so, that a linear relationship between control voltage and frequency existed. Figure 6 is a plot of measured VCO frequency and  $H$  versus control voltage, showing this assumption not to be accurate. Note that  $H$  decreases by more than  $3\frac{1}{2}$  times as the frequency changes from 1238 to 4520 Hz.

Thus, over the indicated frequency range, the loop gain is decreased by a factor of 14 or more.

Gamma, which was assumed to be a constant for purposes of simplifying the derivation of Eq. (9), is given by

$$\gamma = [(\omega R_{21} C_x)^2 + 1]^{1/2}$$

where  $\omega = 2\pi f$  rad/sec.

Using this equation and the measured data from Table 1, we can calculate the results shown in Table 2.

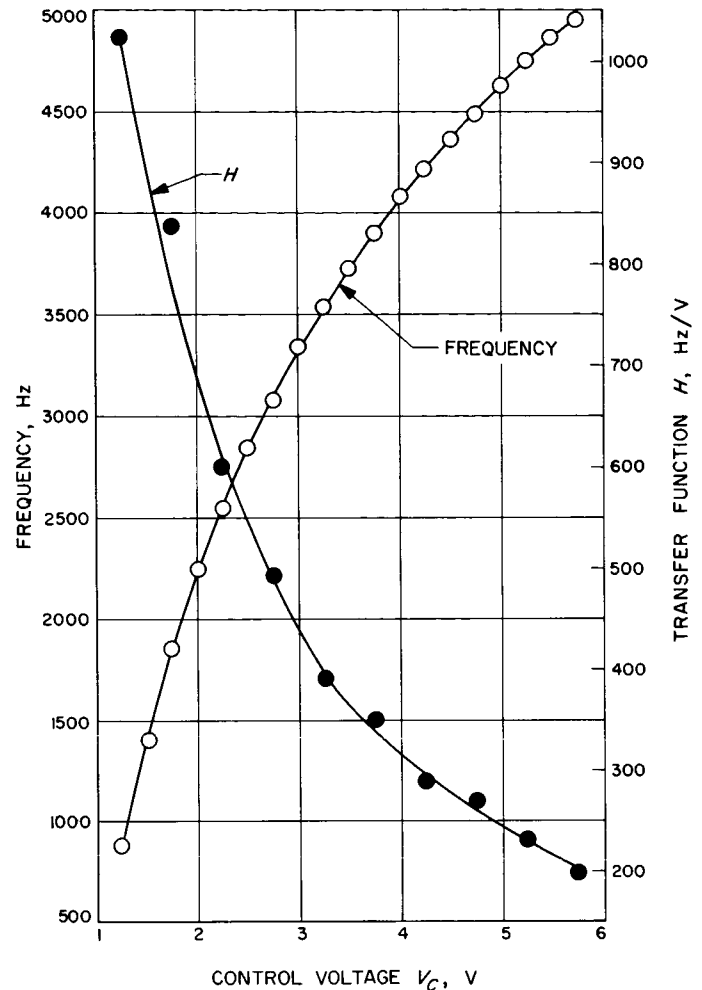


**Fig. 6. Frequency and  $H$  as a function of control voltage**

**Table 2. Variations of  $\gamma$  as a function of frequency<sup>a</sup>**

$C_x$ , pF	$f$ , Hz	$\omega R_{21} C_x$	$\gamma$
2030	4520	0.472	1.10
2531	3710	0.485	1.11
3037	3140	0.490	1.12
4016	2415	0.501	1.12
5045	1942	0.505	1.12
6041	1633	0.509	1.12
7031	1410	0.512	1.12
8042	1238	0.512	1.12

<sup>a</sup>Data taken at 25°C.

Since  $\gamma$  appears in the closed-loop expression of Eq. (9),  $\gamma$  will account directly for a -2% deviation from the idealized theoretical frequency at 4520 Hz.

**Table 3. Instrument calibration and frequency deviation as a function of temperature**

$C_x$ , pF	$\Delta f$ , Hz				$f_{ref}$ , Hz (reference at 25°C)	$\Delta f$ , Hz			Maximum deviation, % ( $\Delta f/f \times 100$ )
	-60°C	-40°C	-20°C	0°C		+50°C	+75°C	+100°C	
8042	-3	+3	+4	+3	1238	-5	-8	-5	-0.65
7031	-4	+3	+5	+4	1410	-5	-9	-6	-0.64
6041	-5	+3	+6	+5	1633	-6	-10	-7	-0.62
5045	-5	+5	+8	+7	1942	-5	-11	-8	-0.57
4016	-5	+7	+10	+8	2415	-7	-14	-11	-0.58
3037	0	+13	+15	+11	3140	-9	-20	-16	-0.64
2531	+10	+21	+22	+16	3710	-12	-25	-23	-0.67
2030	+33	+40	+36	+24	4520	-19	-36	-41	-0.90

### B. Performance vs Temperature

With the temperature extremes of ablative heating and Martian cold as design considerations, this instrument has been designed to operate over the range of -60 to +100°C. A capacitance decade box was used to simulate the aluminum oxide detector so that the performance of the electronic circuitry could be isolated. Table 3 gives (1) the results of a calibration relating instrument frequency to a detector capacitance and (2) the frequency deviations that result as a function of temperature.

Two additional calibrations were performed, with the data taken in the same manner as the data of Table 3. These data, which demonstrate the repeatability of frequency deviation vs temperature, are shown in Table 4.

Thus, if the temperature of the instrument is known, the calibration of the electronics, at any temperature in the range of -60 to +100°C, can be reproduced to within 0.2%.

The thermal deviations that have been noted can be attributed primarily to the VCO frequency control diodes (designated D3 and D4 in Fig. 4), the AGC field effect transistor Q4, and the gain changes in the differential amplifier.

Of these three sources of frequency change, the VCO frequency control diodes are of particular interest. Figure 7 depicts the typical behavior of the diodes as a function of temperature. For a given change in temperature, the diode curve experiences a greater voltage displacement at the knee than it does in the higher current regions. For this reason, the dynamic resistance of the

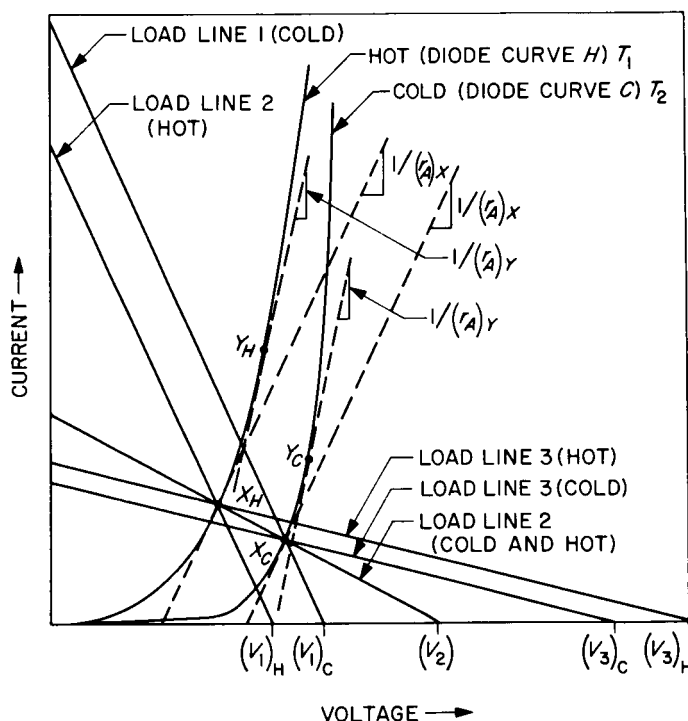


**Fig. 7. Thermal characteristics of the VCO frequency control diodes**

diodes ( $dv/di$ ) is characterized by a positive temperature coefficient.

For a Wien bridge oscillator of the type used in this instrument, the frequency  $f$  is determined by the time constant

$$\tau_A = \frac{1}{2\pi f} = r_A C_A$$

Table 4. The repeatability of frequency deviation vs temperature<sup>a</sup>

$C_x$ , pF	Frequency deviation, Hz								Max ( $\Delta f/f_1$ ), %
	$f_1 - f_2$	$f_1 - f_3$	$f_1 - f_2$	$f_1 - f_3$	$f_1 - f_2$	$f_1 - f_3$	$f_1 - f_2$	$f_1 - f_3$	
8042 7031 6041 5045 4016 3037 2531 2030  8042 7031 6041 5045 4016 3037 2531 2030	From -60 to 0°C								+0.16 +0.07 +0.06 +0.10 -0.09 -0.10 +0.08 +0.07  +0.08 -0.14 +0.06 +0.10 +0.13 +0.16 +0.14 +0.11
	-60°C		-40°C		-20°C		0°C		
	+2	+2	+1	+1	0	0	0	+1	
	+1	+1	0	+1	0	0	0	0	
	+1	+1	0	0	0	+1	0	0	
	0	0	0	+1	+1	+1	0	+2	
	-2	+1	0	+1	0	0	-1	+1	
	-3	+1	+1	+1	+1	0	-1	+1	
	-1	+1	+1	+1	+1	+1	-1	+3	
	+1	+3	0	+1	+1	+2	-1	+3	
	From +25 to +100°C								
	+25°C		+50°C		+75°C		+100°C		
	0	+1	0	+1	0	+1	-1	0	
	-1	0	0	+1	0	0	-1	-2	
	0	0	0	+1	+1	+1	-1	-	
-1	-1	+1	+2	+1	+2	+2	0		
-1	-1	+1	+3	+1	0	-1	0		
-1	-1	+2	+5	0	+1	0	+2		
-1	-1	+2	+5	0	+2	0	+1		
-2	-1	+2	+5	0	+2	+2	+3		

<sup>a</sup>Where  $f_1 - f_2$  is the frequency deviation between the first and second calibration, and  $f_1 - f_3$  is the frequency deviation between the first and third calibration. The data  $f_1$ ,  $f_2$ , and  $f_3$  were taken on three successive days.

These terms are defined in the block diagram of Fig. 8. Through the use of forward-conducting diodes for  $r_A$  and  $r_B$ , the frequency is controlled by operating at the appropriate point on the diode curve. As the diode curve  $H$  of Fig. 7 shows, operation at point  $X$  produces a lower frequency than operation at point  $Y$ , since the slope at  $Y$  is greater than it is at  $X$ .

For a given water vapor concentration, the aluminum oxide detector will assume a capacitance  $C_x$  having one characteristic frequency at a given temperature. Assume that this temperature is the one that produces diode curve  $H$  of Fig. 7. If the temperature then decreases so as to modify the diode curve to the new shape of diode curve  $C$ , the VCO would temporarily want to operate at a different frequency because of the decreased resistance in  $r_A$ . But the new frequency would unbalance the bridge containing  $C_x$ , creating an error voltage. This

error voltage is then amplified by the differential amplifier and applied to the series combination of  $R_{35}$  and the control diodes  $D_3$  and  $D_4$ . The loop thus seeks to return to its original frequency, but since an incremental change in control voltage is required to change the operating point on the diode curve, the new steady-state frequency will be in error by the amount necessary to provide that increment.

Referring to Fig. 7, it will be seen that the magnitude and sign of the error signal depend on (1)  $R_{35}$ , which determines the slope of the load line, (2) the region of the curve, which determines the frequency, and (3) the shape of the diode curve, which generally varies from one diode to the next.

First, consider operating at point  $X_H$  (low-frequency case). When the temperature has decreased to  $T_2$ , the

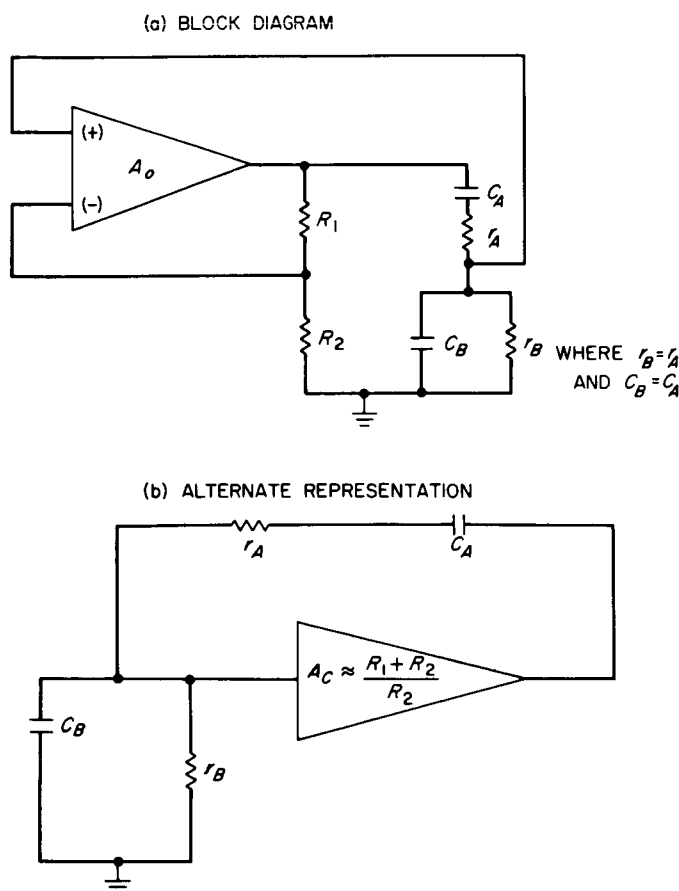


Fig. 8. The Wien bridge oscillator

diode current must be decreased so as to allow operation at point  $X_c$ . If  $R_{35}$  is chosen to require operation along load line 1, the error signal must cause the control voltage to increase from  $(V_1)_H$  to  $(V_1)_c$ ; along load line 2, no change in voltage is required; and load line 3 necessitates a decrease in voltage from  $(V_3)_H$  to  $(V_3)_c$ .

Going up the curve to point  $Y_H$  (region of higher frequency,  $(V_A)_X > (V_A)_V$ , with the same change in temperature  $T_1$  to  $T_2$ ) requires a larger change in diode current to keep  $V_A$  at the same value. But now the error signal is required to decrease the control voltage, regardless of which of the three load lines is chosen. It should be noted, though, that  $R_{35}$  could be chosen small enough that the polarity of the error signal could be reversed, which corresponds to an incremental frequency change of the opposite polarity.

As a final comment, it should be mentioned that the main limitation in minimizing thermal frequency deviations is dictated by loop gain considerations. It was discussed in the previous section that at room temperature

the loop gain decreases by a factor of more than 14 in going from the low to the high end of the frequency range. Further increases and decreases in loop gain are caused by temperature changes. Thus, in making the loop tight and minimizing thermal frequency deviation at the high-frequency end, the gain and phase margins are narrowed at the low-frequency end.

### C. Processing the Error Signal

In the general description of the instrument, it was stated that the bridge voltages  $e_N$  and  $e_R$  of Fig. 1 must first be rectified and filtered before being amplified by the differential amplifier. To understand the necessity of this requirement, refer to Fig. 9. The vector diagram makes use of the fact that voltage across the resistor ( $e_R$ ) leads the voltage across the capacitor ( $e_C$ ) by 90 deg and that the vector sum of the resistor voltage  $e_R$  and detector voltage  $e_C$  must remain equal to  $e_o$ , which is a constant. Therefore, from elementary geometry, we know that the locus of  $e_N$  describes a semicircle as  $e_C$  goes from 0 to  $e_o$ .

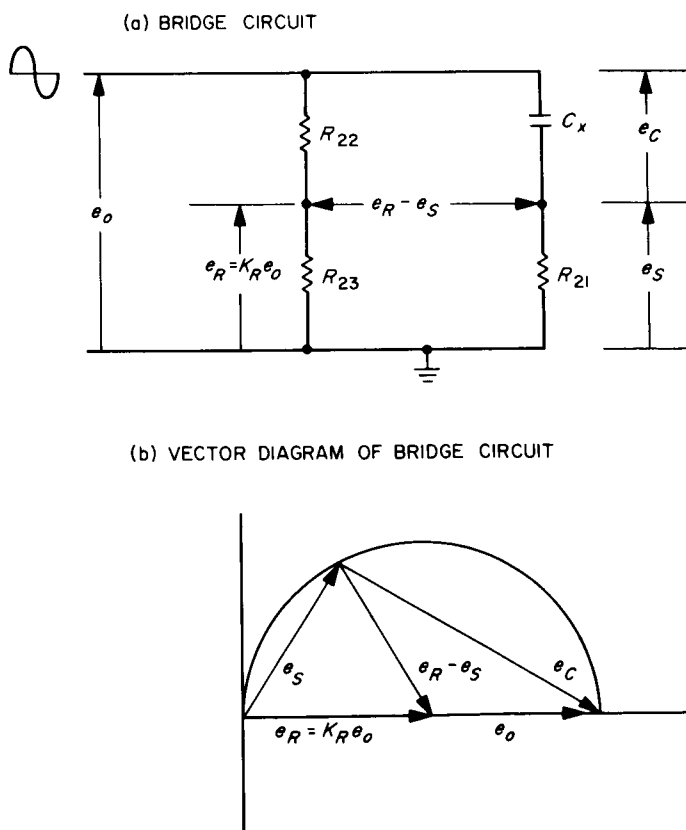


Fig. 9. Bridge circuit and vector diagram



From this construction it can be seen that the error signal ( $e_R - e_S$ ) never approaches null, except for the meaningless case when  $K_R = 1$  and  $e_C = 0$ . To make null possible, only the magnitudes of  $e_R$  and  $e_S$  must be differenced. To accomplish this,  $e_S$  and  $e_R$  are rectified using the base-emitter actions of a matched dual-transistor (Q9AB). This technique has two advantages over the use of diodes: (1) Only base current need be supplied to the transistor (therefore, the rectifying action has negligible loading effect), and (2) because the thermal changes in  $V_{BE}$  are matched, spurious error signals due to  $\Delta V_{BE}$  are minimized.

#### D. The Power Supply

The power supply provides  $\pm 18$  V. It consists of a current limiter, a dc-to-ac converter, a full-wave rectifier and filter, and a series regulator. A schematic of the system is shown in Figs. 10 and 11.

The building blocks of the system are of conventional design, with primary effort directed towards minimizing components while still achieving tight regulation versus temperature and input voltage variations. Minimization of components was realized by regulating the center tap on the primary of the converter, rather than individually regulating the  $\pm 18$ -V outputs.

A simplified diagram of the voltage regulator is shown in Fig. 12, from which the parameters of main importance may be determined. To study these parameters, an expression for the output voltage will now be derived. Thus

$$V_P \gamma = h_{FE_1} h_{FE_2} i_b R_L \quad (13)$$

where

$$V_P = \text{the nominal } +18 \text{ V}$$

$$V_P \gamma = \text{the voltage seen at the center tap of the converter's primary}$$

$$h_{FE_1}, h_{FE_2} = \text{the respective forward transfer ratios of transistors Q3 and Q4 (Fig. 10)}$$

$$R_L = \text{the load seen at the center tap of transformer T2, from the primary side}$$

$$i_b = I_K - G_m (KV_P - E_R) \quad (14)$$

where

$$I_K = \text{a constant current from the constant-current source Q5}$$

$$G_m = \text{the transconductance of the differential amplifier (Q6AB)}$$

$$K = \text{the voltage divider action of R7 and R8}$$

$$E_R = \text{the reference voltage fixed by D12}$$

Then substituting Eq. (14) into Eq. (13) and solving for  $V_P$  results in

$$V_P = \frac{h_{FE_1} h_{FE_2} (I_K + G_m E_R) R_L}{\gamma \left( 1 + \frac{h_{FE_1} h_{FE_2} G_m K R_L}{\gamma} \right)} \quad (15)$$

Typical values for these parameters are

$$h_{FE_1} = 150$$

$$h_{FE_2} = 60$$

$$I_K = 100 \mu\text{A}$$

$$G_m = 1.1 \text{ mA/V}$$

$$E_R = 6.5 \text{ V}$$

$$\gamma = 0.95$$

$$K = 0.36$$

$$R_L = 1.2 \text{ k}\Omega$$

By substituting these values into Eq. (15), it can be seen that

$$\frac{h_{FE_1} h_{FE_2} G_m K R_L}{\gamma} \gg 1$$

Therefore,

$$V_P \approx \frac{I_K}{G_m K} + \frac{E_R}{K} = 0.28 + 18$$

The reference voltage and divider ratio are therefore of principal importance in determining the regulation. Of secondary importance are the current source and the differential amplifier. It should be noted that both  $E_R$  and  $I_K$  are functions of Zener reference diodes and that these diodes, therefore, are the limiting factors in the circuit's thermal performance.

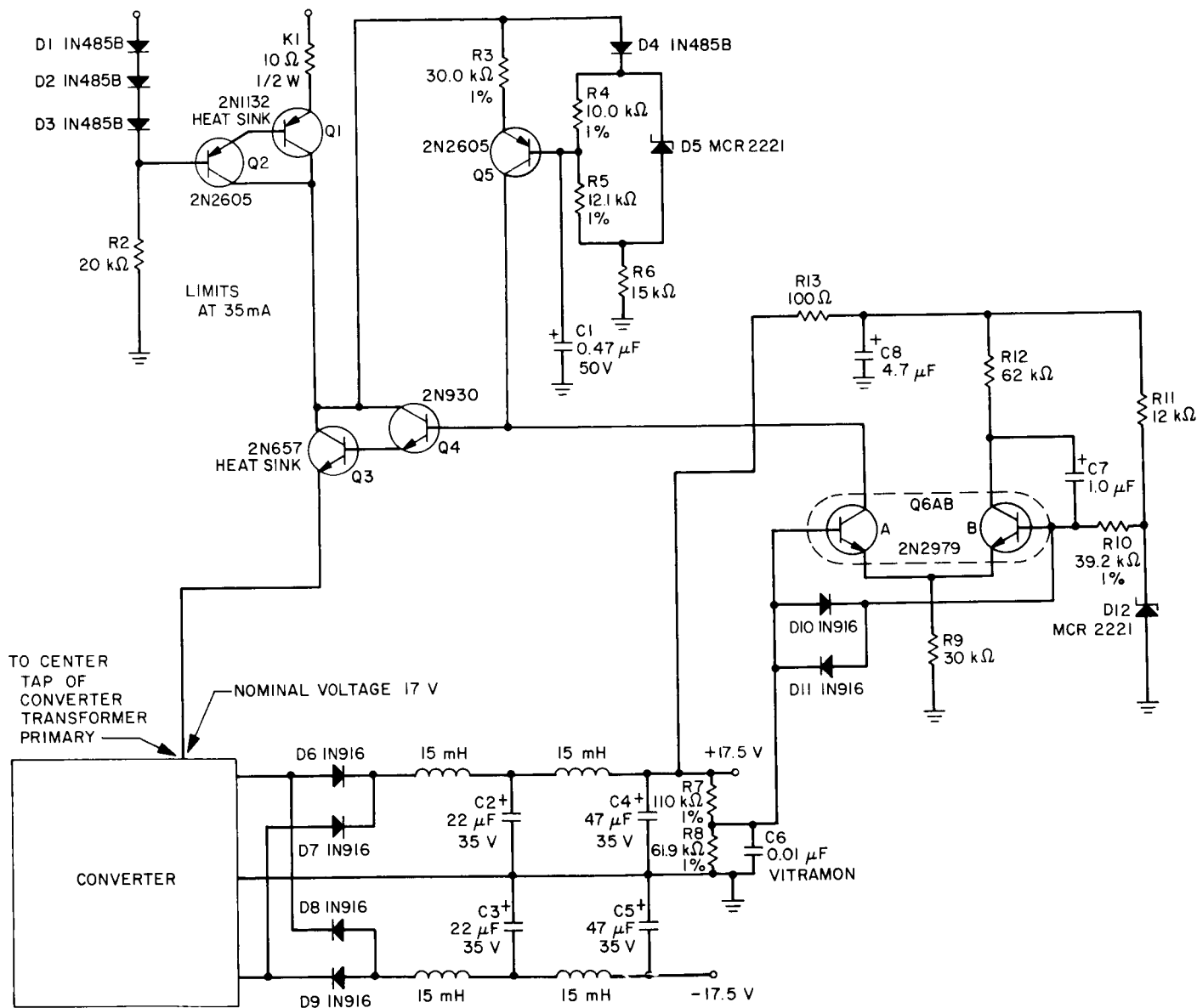


Fig. 10. Water-detection power conversion and regulator system

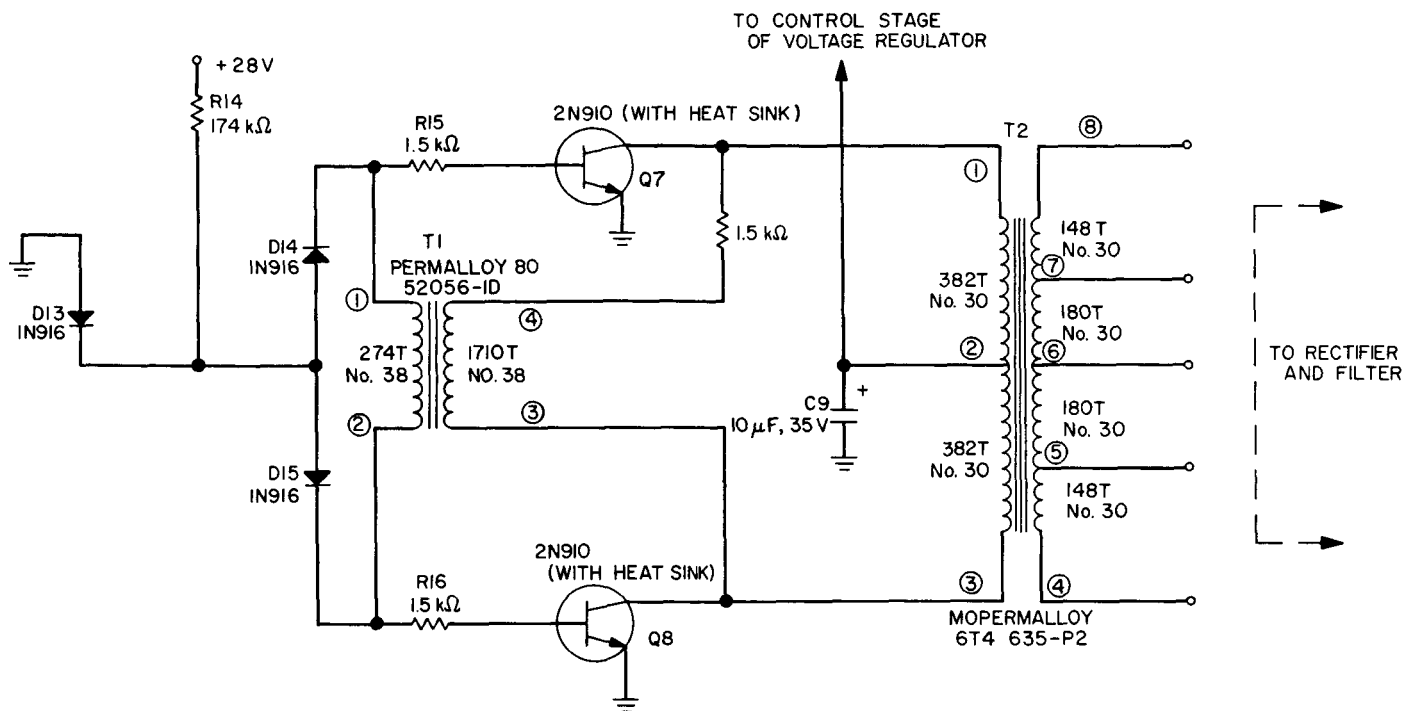


Fig. 11. Converter (dc to ac)

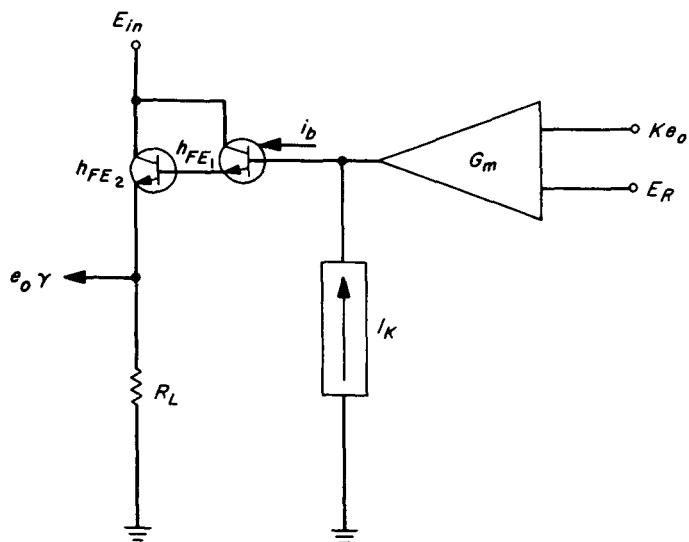


Fig. 12. Simplified diagram of the voltage regulator

#### IV. Conclusion

The schematics and data presented in this report are representative of what has been done using discrete components. Within this framework the raw power required by the complete instrument is less than 0.4 W, and it can be reasonably assumed that the instrument would weigh approximately 0.8 lb and occupy less than 36 in.<sup>3</sup> in a flight configuration.

In addition to the work that has been described, a second-generation version of this system (minus the power supply) has been built using integrated circuits. Initial observations of its performance indicate that it works as well as the discrete-component version, if not better. The power required for its operation is comparable to that of the discrete-component version, and it is anticipated that the weight and volume of the total instrument can be cut to one-half that of the first-generation instrument.

## Nomenclature

A1	ac amplifier	$I_K$	collector current of power supply transistor Q5
$A_1$	voltage gain of amplifier A1	$K$	power supply divider ratio of R7 and R8
A2	differential dc amplifier	$K_R$	bridge divider ratio of R22 and R23
$A_2$	voltage gain of amplifier A2	$K_N$	bridge divider ratio of $C_x$ and R21
$C_A$	capacitance of C7	$r_A$	dynamic forward resistance of diode D3
$C_x$	capacitance of the aluminum oxide water vapor detector	$R_L$	power supply reflected load impedance seen at the center tap of the primary of transformer T2
$e_C$	instantaneous voltage across the aluminum oxide water vapor detector	R21	resistor in bridge circuit R-C divider
$e_o$	instantaneous output voltage of amplifier A1	R22	resistor in bridge circuit resistive divider
$e_R$	instantaneous resistive divider voltage ( $e_R = K_R e_o$ )	R23	resistor in bridge circuit resistive divider
$e_N$	instantaneous R-C divider voltage ( $e_N = K_N e_o$ )	$V_C$	VCO control voltage
$E_o$	peak value of $e_o$	$V_o$	output voltage of A2 for $\epsilon = 0$
$E_R$	Zener reference voltage of D12	$V_P$	positive regulated output voltage of system power supply
$f$	VCO output frequency	$V_R$	rectified and filtered value of $e_R$
$f_{ref}$	calibration frequencies as a function of $C_x$ at 25°C	$V_N$	rectified and filtered value of $e_N$
$\Delta f$	incremental change of frequency	$\gamma \equiv [(\omega R_{21} C_x)^2 + 1]^{1/2}$	
$f_1$	first set of calibration frequencies	$\epsilon$	input error signal into A2
$f_2$	second set of calibration frequencies	$\eta_A \equiv V_N / (e_{N_{max}} - V_{BEA})$	
$f_3$	third set of calibration frequencies	$\eta_B \equiv V_R / (e_{R_{max}} - V_{BEB})$	
$F$	frost point in °C	$\pi \equiv 3.14 \dots$	
$G$	loop gain of the H <sub>2</sub> O detection electronics	$\tau_A = r_A C_x$	Wien bridge time constant
$H$	VCO transfer function relating output frequency $f$ to control voltage $V_C$	$\omega$	frequency in radians/second